energy&fuels

ARTICLE

pubs.acs.org/EF

Ab initio-based Mercury Oxidation Kinetics via Bromine at Postcombustion Flue Gas Conditions

Jennifer Wilcox[†,*] and Terumi Okano[†,‡]

[†]Stanford University, Department of Energy Resources Engineering, 367 Panama Street, Green Earth Sciences, Stanford, California 94305, United States

[‡]Ze-gen, Inc., 1380 Soldiers Field Road, Second Floor, Boston, Massachusetts 02135, United States

ABSTRACT: Because direct mercury measurements are difficult throughout the postcombustion flue gas environment, it is practical to use mercury reaction kinetics to theoretically determine mercury speciation based upon coal composition, plant equipment, and operating conditions. Elemental mercury cannot be captured in wet scrubbers; however, its oxidized forms can. Mercury−bromine oxidation kinetics have been studied with electronic structure calculations using a broad range of ab initio methods. Reaction enthalpies, equilibrium bond distances, vibrational frequencies, and rate constants have all been predicted using density functional theory as well as coupled cluster methods. Upon the basis of comparisons to available experimental and high-level theoretical data in the literature, quantum-based methods for the following Hg−Br reactions have been validated: Hg + Br ↔ HgBr, Hg + Br_2 ↔ HgBr + Br, and HgBr + Br ↔ $HgBr_2$. The use of these methods for predicting forward and reverse rate constants for the following Hg−Br reactions has been carried out for the first time: Hg + HBr ↔ HgBr + H, HgBr + Br_2 ↔ $HgBr_2$ + Br, and HgBr + HBr ↔ $HgBr_2$ + H. Understanding the speciation of mercury in the flue gases of coal combustion is paramount to the development of efficient control technologies.

INTRODUCTION

The release of the toxic trace metal, mercury (Hg), has long been a significant issue for coal-fired power plants, which must implement flue gas scrubbing to prevent Hg emissions into the atmosphere. Unlike its oxidized forms, Hg^{2+} and Hg^{+}, elemental mercury cannot be captured in wet scrubbers. Bromine has been found to effectively oxidize Hg from pilot- and full-scale tests carried out by the US Department of Energy.[1] Other field studies have shown bromine to be effective in Hg removal from coal-fired boilers, and a bromine additive technology has recently been implemented in several companies to enhance Hg oxidation.[2] In addition, it has recently been shown that direct bromine gas injection can effectively convert elemental mercury (Hg^0) to oxidized mercury (Hg^{2+}, Hg^{+}).[3] Since capture technologies are highly dependent upon the form of Hg that is present, investigations regarding their speciation are extremely important. Understanding the kinetic and thermodynamic behavior of Hg from the high to low temperature regime will allow for increased model accuracy in predicting its complicated speciation, which in turn will facilitate the design and application of more effective Hg control devices. More specifically, these rate data can be used in the creation of a mercury−bromine mechanism that currently does not exist for postcombustion environment applications.

Though there have been numerous efforts to study Hg compounds that are relevant to atmospheric studies, there is little data currently available for Hg compounds present in postcombustion flue gases. There are limited experimental and theoretically derived rate data available in the literature for modeling mercury−bromine reactions over a broad temperature range applicable to the quenching region of coal-fired flue gases. The current work presents an ab initio study of the forward and reverse reaction kinetics of the following three first-stage and three second-stage oxidation reactions of Hg with bromine (Br) and hydrogen (H) compounds likely present in coal-fired flue gases:

$$Hg + Br \leftrightarrow HgBr \quad (R1)$$

$$Hg + Br_2 \leftrightarrow HgBr + Br \quad (R2)$$

$$Hg + HBr \leftrightarrow HgBr + H \quad (R3)$$

$$HgBr + Br \leftrightarrow HgBr_2 \quad (R4)$$

$$HgBr + Br_2 \leftrightarrow HgBr_2 + Br \quad (R5)$$

$$HgBr + HBr \leftrightarrow HgBr_2 + H \quad (R6)$$

Experimental kinetic parameters are available only for forward directions of R1[4−8] and R2.[7] The forward rate constant for R1 has been calculated theoretically by Shepler et al.,[4] Khalizov et al.,[5] Spicer et al.,[6] and Ariya[7] with the reverse predicted from theory by Shepler at al.[4] and Goodsite et al.[9] Shepler et al.[4] calculated kinetic parameters from ab initio calculations and quasiclassical trajectories using argon as the bath gas. Khalizov et al.[5] used canonical variational transition state theory (CVTST)[10] to calculate the rate parameters, but only at the high-pressure limit and at low temperature. Goodsite et al.[9] used Rice−Ramsperger−Kassel−Marcus (RRKM)[11] theory along with the hybrid density functional Hartree−Fock B3LYP[12,13]

Received: December 29, 2010
Revised: February 18, 2011
Published: March 16, 2011

method and a similar approach to predict the forward kinetics of R4. The forward and reverse kinetics of R2 and R4 have been predicted by Balabanov et al.[14] using the internally contracted multireference configuration interaction (including single and double excitations) method with the augmented correlation consistent basis sets, aug-cc-pV*n*Z-PP (n = 2, 3, 4) for calculating the reaction rates. Within all of these previous studies, the reaction conditions were outside of the range of interest for postcombustion flue gas studies, having all been carried out at 1 atm and at temperatures at or below 400 K. To the authors' knowledge, there have been no experimental or theoretical investigations carried out for R3, R5, and R6.

In the current work, kinetic data is predicted over a temperature range of 298−2000 K, representative of postcombustion flue gas conditions. RRKM theory is used for the two unimolecular reactions, and VTST, for the bimolecular reactions. Calculations were carried out using the MOLPRO[15] suite of ab initio programs.

THEORETICAL METHODOLOGY

Ab initio Calculations. Before the kinetic parameters could be calculated, it was necessary to determine which level of theory would be the most accurate for the Hg compounds through a comparison of geometries, vibrational frequencies, and heats of reaction predictions to available experimental data. In the case of R1, R2, and R4, kinetic data is available for direct comparison at low temperature (i.e., less than 400 K). All reactions were investigated using using the coupled cluster singles and doubles method including triple excitations (CCSD(T))[16−18] with the Aug-cc-pVTZ[19,20] basis set. The augmented correlation consistent basis sets of triple-ζ quality (Aug-cc-pVTZ-PP, shortened to AVTZ) incorporating scalar relativistic effects were employed through the use of small-core relativistic pseudopotentials (PP)[21] for the inner electrons of Hg and Br. This same basis set was employed for H, but without a pseudopotential.

In addition to CCSD(T)/AVTZ, the B3LYP method was tested with three different basis sets. The first basis set employed was LANL2DZ,[22] which uses an all-electron description for atoms of the first row elements, and an ECP for inner electrons combined with double-ζ quality functions to describe the valence electrons on heavier atoms of elements such as Hg. The second basis set employs a relativistic compact effective potential, RCEP60VDZ of the Stevens et al. group,[23] which replaces 60 of Hg's atomic core electrons and is derived from numerical Dirac−Fock wave functions using an optimizing process based upon the energy-overlap functional. Energy-optimized (8s8p5d)/[4s4p3d] Gaussian-type double-ζ quality sp and triple-ζ quality d functions were used for Hg, with the triple-ζ d functions essential for describing the orbital shape changes that exist with d occupancy. The third basis set employs the ECP60MDF effective core potential of the Stuttgart group[21] with the energy-optimized (8s8p7d)/[6s6p4d] Gaussian-type orbital (GTO) valence basis optimized using multiconfiguration Dirac−Fock (MCDF) calculations. An extended triple-ζ Pople[24] basis set, 6-311G*, including the addition of a single polarization function was used for Br and H atoms in conjunction with the RCEP60VDZ and ECP60MDF basis sets used for Hg.

Kinetic Calculations. To determine the unimolecular decomposition rate constants for R1 and R4, RRKM theory was carried out using the Holbrook et al.[25] text on unimolecular reactions as a guide. RRKM theory models a unimolecular decomposition reaction as a two-step process following the general form shown in R7 where AB is the reactant molecule, M is the collision partner, and * indicates that the species is energized.

$$\begin{aligned} \mathrm{AB} + \mathrm{M}^* &\overset{k_1}{\leftrightarrow} \mathrm{AB}^* + \mathrm{M} \\ \mathrm{AB}^* &\xrightarrow{k_a} \mathrm{A} + \mathrm{B} \end{aligned} \tag{R7}$$

The overall rate constant expression, k_{uni}, is given in eq 1, in which the rate constants of both the deactivation (first step of R7) and the decomposition (second step of R7) are taken into account:

$$k_{uni} = \frac{LQ_1^+}{N_a h Q_1 Q_2} e^{[-E_0/RT]} \Delta E \sum(X) \tag{1}$$

In eq 1, the statistical factor, L, is the number of possible ways the reaction can proceed to obtain a desired product. For instance in the case of HgBr decomposition, L = 1 since there is only one way in which the species can dissociate into Hg and Br atoms. The quantity Q_1^+ is the rotational partition function of the adiabatic rotations of the activated complex, Q_1 is the rotational partition function of the reactant, and Q_2 is the vibrational partition function of the reactant. Additionally, E_0, the activation barrier, is the difference between the minimum energy required to cross the barrier and the reactant energy, while E^* is the energy of each state relative to E_0, and ΔE is the step size between states. The sum over states, X, is defined as

$$X = \frac{W}{1 + \dfrac{k_a}{\beta_c Z_{LJ}[\mathrm{M}]}} e^{[-(E^* - E_0)/RT]} \tag{2}$$

such that

$$k_a = \frac{L}{N_a h} \frac{Q_1^+}{Q_1} \frac{W}{\rho} \tag{3}$$

The deactivation rate constant is represented by the $\beta_c Z_{LJ}[\mathrm{M}]$ term, while the decomposition rate constant, k_a, is given by eq 3. The collisional efficiency factor, β_c, was set equal to 0.1, as the reactions were assumed to be in an inert bath gas,[26] and [M] is simply the concentration of the collision partner. The equation for the Lennard-Jones parameter (eq 2) is as follows:

$$Z_{LJ} = N_a \sigma_{am}{}^2 \sqrt{\frac{8RT}{\pi \mu_{am}}} \Omega_{am} \tag{4}$$

such that

$$\Omega_{am} = \left[0.636 + 0.567 \log\left(\frac{kT}{\varepsilon_{am}}\right)\right]^{-1}, \text{when } 0.3 \le \frac{kT}{\varepsilon_{am}} \le 500 \tag{5}$$

$$\Omega_{am} = \left[0.697 + 0.5185 \log\left(\frac{kT}{\varepsilon_{am}}\right)\right]^{-1}, \text{when } 3 \le \frac{kT}{\varepsilon_{am}} \le 300 \tag{6}$$

and

$$\frac{\varepsilon_{am}}{k} = 65.3 T_c Z_c{}^{18/5} \tag{7}$$

Within eq 4, μ represents the reduced mass, and σ, the collision diameter, in which the subscript "am" refers to the

Table 1. Comparison between Experimental and Theoretical Vibrational Frequencies and Bond Lengths for Molecules Involved in R1−R6 for Three Levels of Theory[a]

	Vibrational Frequencies (cm^{-1})			
	experiment	B3LYP/LANL2DZ	B3LYP/ECP60MDF	CCSD(T)/ AVTZ
HBr	2650[b]	−249.75	−107.92	*-5.59*
Br_2	325.3[c]	−54.84	−14.96	*-11.02*
HgBr	188.3[d]	−21.83	−34.43	*-25.60*
	218[e]; 220[f]			
$HgBr_2$ (symmetric stretch)	222[g]; 229[h]	−40.2 to −51.2	−16.6 to −27.6	*0.25* to *10.75*
(bend)	68[i]	−19.9	−7.97	*-0.45*
(asymmetric stretch)	293[j]	−49.2	−21.4	*-3.40*

	Bond Length (Å)			
	experiment	B3LYP/LANL2DZ	B3LYP/ECP60MDF; (RCEP60VDZ)	CCSD(T)/AVTZ
HBr	1.41[k]	0.05	0.02	*0.01*
Br_2	2.28[c]	0.23	0.05	*0.03*
HgBr	2.62[d]	0.16	*0.02* (0.005)	0.08
$HgBr_2$	2.37[l]	0.14	0.09 (0.09)	*0.03*

[a] Deviations are represented in inverse centimeter and angstroms for the vibrational frequency and bond length prediction data, respectively. [b] Reference 35. [c] References 31 and 32. [d] Reference 33. [e] Reference 37. [f] Reference 36. [g] Reference 39. [h] Reference 38. [i] Reference 40. [j] Reference 41. [k] References 30 and 31. [l] Reference 34.

reactant molecule, A, and the collision partner, M. In determining the Lennard-Jones parameter, a correction factor, Ω, is also used and is calculated using either eq 5 or 6. The value of ε_{am}/k is found along with the eq 7 using critical temperature and compressibility data.

The energy level consists of a series of steps above that of the transition structure, as predicted by the Lindemann−Hinshelwood mechanism;[11] the number of steps for any given reaction will depend upon the step size, ΔE, and the maximum energy, E_{max}. These are both selected arbitrarily but ΔE is typically between 0.4 and 2.0 kJ/mol[24] (30−170 cm^{-1}), while E_{max} was set equal to 9000 cm^{-1}.

Once the values of ΔE and E_{max} are determined, the sum and density of states are calculated at each energy level using the Beyer−Swinehart algorithm.[27] This algorithm predicts how many linear combinations of vibrational frequencies, i.e., states that exist between E_0 and E_{max}, and determines which energy level they exist at based upon their magnitude, and energy range will then have a number of states associated with it. The density of states, ρ, for each range is the number of states divided by the step size, ΔE, while the sum of states, W, is a direct count of how many states exist at or below the current energy level. By finding W and ρ at each energy level, the value of k_a at the corresponding levels can be determined followed by the overall sum of the quantity X used in calculating the rate constant, k_{uni}. The forward second-order rate constant expressions for atom−radical recombination R1 and radical−radical recombination R4 were calculated using the product of the reverse RRKM-derived rate constant and the experimental equilibrium constant, K_{eq}.[28]

For bimolecular R2, R3, and R5, variational transition state theory was used, and for R6, traditional transition state theory was used, both including the Wigner[29] tunneling correction factor, represented below by eqs 8 and 9, respectively:

$$k^{TST} = \frac{k_b T}{h}\frac{Q_{TS}}{Q_1 Q_2} e^{(-E_a/RT)} \quad (8)$$

and

$$k_T = 1 + \frac{1}{24}\left[\frac{hcv}{k_b T}\right]^2 \quad (9)$$

such that

$$k = k^{TST} k_T \quad (10)$$

In eq 8, E_a is the activation barrier, and Q_{TS}, Q_1, and Q_2 are the total partition functions of the transition structure and reactant species 1 and 2, respectively. Within the Wigner tunneling correction factor (eq 9), ν represents the single imaginary frequency value of the transition structure, and the product of k^{TST} and k_T equate to the total bimolecular rate constant. The use of the Wigner tunneling correction is questionable for light species, and in future work a more rigorous tunneling correction for the reactions involving H and HBr should be employed. This methodology was carried out for both forward and reverse directions of the bimolecular reactions of focus. In the case of VTST, different dividing surfaces perpendicular to the reaction coordinate were considered. For instance, in each of the reactions, the distance between Hg and Br atoms was varied and the rate constant was calculated for each distance considered, with the final rate constant chosen corresponding to the minimum. Potential energy surfaces comprised of approximately 200 single-point energies were generated without energy corrections. Zero-point corrections were added to the reactant, transition structure, and product energy values over the 298−2000 K temperature range. Partition functions and corresponding rate constants were calculated as a function of temperature to arrive at general forward and reverse rate constant expressions as described in further detail in the Results and Discussion section.

RESULTS AND DISCUSSION

Theoretical geometries and vibrational frequency data have been predicted for the following species: $HgBr_2$, HgBr, HBr, and Br_2. They are compared against experimental data in Table 1.

Table 2. Comparison between Experimental and Theoretical Reaction Enthalpies (kcal/mol) at 298.15 K and 1 atm for Three Levels of Theory[a]

	experiment[b]	B3LYP/LANL2DZ	B3LYP/ECP60MDF; (RCEP60VDZ)	CCSD(T)/ AVTZ
R1 Hg + Br ↔ HgBr	−16.51	−2.04	−7.66 (−0.21)	0.77
R2 Hg + Br_2 ↔ HgBr + Br	29.56	−18.27	−8.18 (−0.73)	2.03
R3 Hg + HBr ↔ HgBr + H	70.95	−12.63	−10.71 (−3.26)	4.57
R4 HgBr + Br ↔ $HgBr_2$	−72.02	18.29	1.89 (7.05)	*0.08*
R5 HgBr + Br_2 ↔ $HgBr_2$ + Br	−25.95	2.06	1.37 (6.53)	*1.34*
R6 HgBr + HBr ↔ $HgBr_2$ + H	15.44	7.70	*-1.16* (−4.00)	3.88

[a] The theoretical values are expressed as a kilocalorie per mole deviation from experiment. [b] Experimental data for Hg species from NIST;[44] data for other species taken from refs 45 and 46.

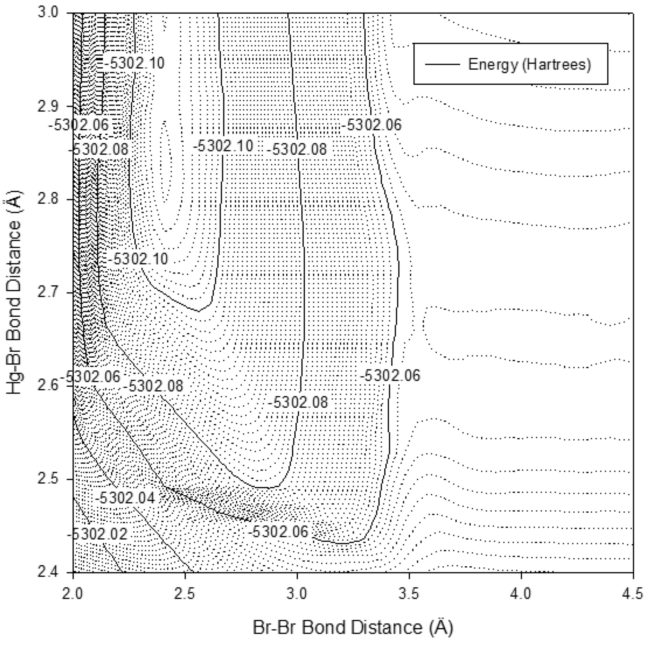

Figure 1. Potential energy surface for R2, Hg + Br_2 ↔ HgBr + Br, at the B3LYP/RCEP60VDZ level of theory.

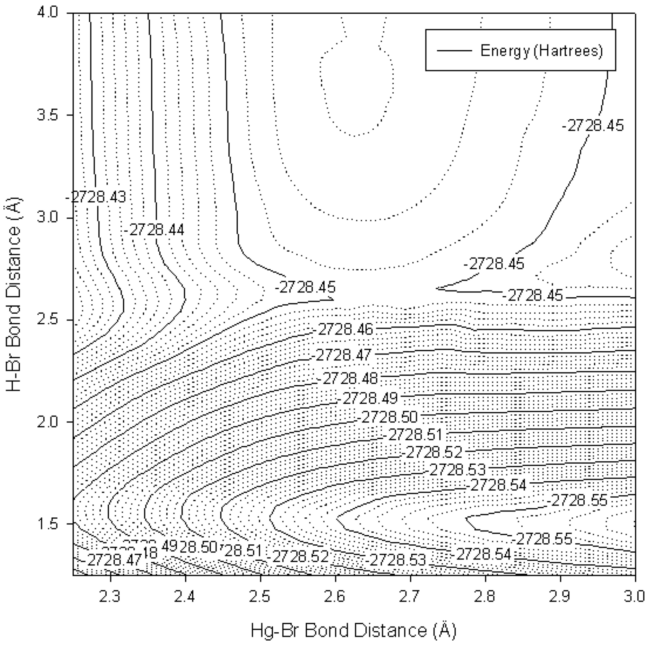

Figure 2. Potential energy surface for R3, Hg + HBr ↔ HgBr + H, at the B3LYP/RCEP60VDZ level of theory.

Experimental methods have yielded bond lengths of 1.414[30,31] and 2.281 Å,[31,32] for HBr and Br_2, respectively. In both cases, the CCSD(T)/AVTZ is the most accurate level of theory of the four investigated in the current work, deviating 0.01 and 0.03 Å from experiment, respectively. The smallest deviations have been italicized in Table 1, and in nearly all cases, with the exception of HgBr, the CCSD(T)/AVTZ level of theory provides the most accurate predictions. The HgBr bond distance was measured by Tellinghuisen and Ashmore[33] using emissions spectra photography, estimating a bond distance of 2.62 Å, which deviates 0.02 and 0.08 Å from predictions at the B3LYP/ECP60MDF and CCSD(T)/AVTZ levels of theory, respectively. Experimental results of Deyanov et al.[34] yield a bond distance of 2.378 Å for the Hg−Br distance in the linear $HgBr_2$ molecule, deviating 0.03 Å from predictions at the CCSD(T)/AVTZ level of theory.

A number of experimental studies are available for the measured vibrational frequencies of each of the species involved, including Br_2,[31,32] HBr,[35] HgBr,[33] and $HgBr_2$.[36−41] In this case, the CCSD(T)/AVTZ level of theory provided the most accurate predictions to the experimental vibrational frequency data, which are represented in parentheses, with the following deviations from experiment: HBr −5.59 (2650[35]), Br_2 −11.02 (325.3[31,32]), HgBr −25.60 (188.3[33]), and $HgBr_2$ 0.25 (218[37]), −0.45 (68[40]), −3.40 (293[41]) cm^{-1}.

In addition to geometric and vibrational spectroscopy data, experimentally derived heats of reaction have also been compared against theoretical predictions at 298 K as shown in Table 2 at the four levels of theory previously described. For R1−R3, the B3LYP/RCEP60VDZ level of theory predicted the most accurate heats of reaction with an underprediction of 0.21, 0.73, and 3.26 kcal/mol for R1, R2, and R3, respectively. The CCSD(T)/AVTZ level of theory most accurately predicted the heat of reaction for R4 and R5 with overstimations of 0.08 and 1.34 kcal/mol, respectively. For R6, the B3LYP/ECP60MDF level of theory predicted the heat of reaction most accurately with an underprediction of 1.16 kcal/mol. Previous investigations of Balabanov and Peterson[42] included energetic contributions beyond the zero-point corrections included in the current work. For instance, they included a core−valence correlation contribution, a scalar relativity correction, a correction for the pseudopotential approximation, and a spin−orbit correction to their

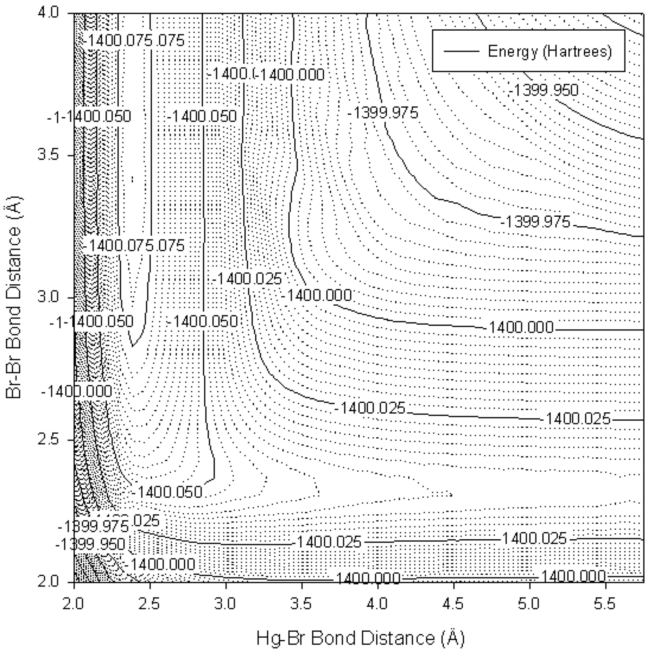

Figure 3. Potential energy surface for R5, $HgBr + Br_2 \leftrightarrow HgBr_2 + Br$, potential energy surface at the CCSD(T)/AVTZ level of theory.

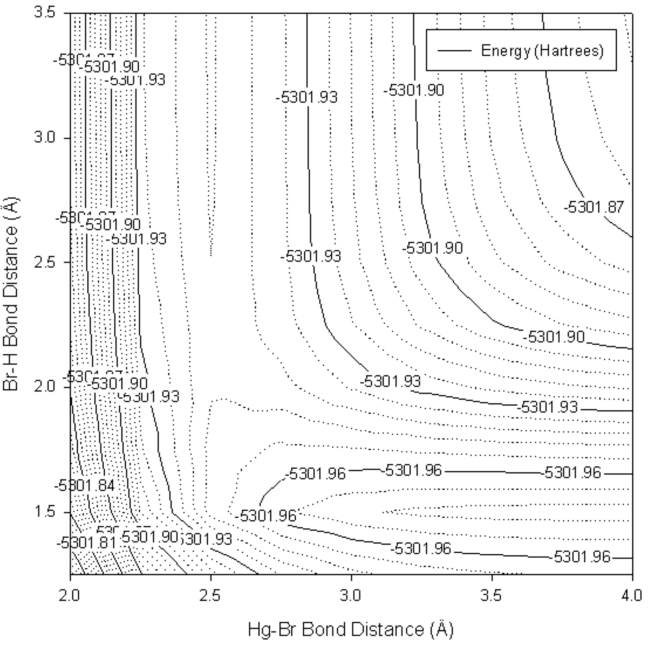

Figure 4. Potential energy surface for R6, $HgBr + HBr \leftrightarrow HgBr_2 + H$, at the B3LYP/ECP60MDF level of theory.

ground-state energy predictions at 0 K. From their work it was shown that in the enthalpies of reaction for those containing Br radical, the contribution from the corrections accounts for approximately 3.5 kcal/mol. The exclusion of these energy correction contributions in the current work will likely influence the energetics of the reactant, product, and activated complex species and could result in increased accuracy if included. Rigorous treatment of the inclusion of these energy corrections will be included in future work. The ultimate goal of the current work is to provide forward and revese kinetic data for R1−R6 over a broad temperature range indicative of postcombustion flue gas conditions.

For R1, R2, and R4, kinetic data exists in the literature, but only at low temperatures applicable to tropospheric conditions, as Hg accumulation in Arctic regions has been shown to influence ozone depletion events through competing reactions with bromine radicals released from sea ice upon exposure to UV light.[43] The forward and reverse rate constants for R1, R2, and R4 are compared against other theory predictions and available experimental data in Table 3. All comparisons made in Table 3 are at 298 K and 1 atm conditions, and the units of the rate constants within Table 5 are cubic centimeters per molecule second, which are traditional units presented in the literature for atmospheric applications. For the forward atom−radical recombination R1, the CCSD(T)/AVTZ value (6.38×10^{-13} cm^3/molecule·s) agrees well with the other theoretical data published, which range from 3.0×10^{-13} to 3.2×10^{-12} cm^3/molecule·s. Donohoue et al.[8] have reported an experimental value of $3.6 \pm 1.8 \times 10^{-13}$ cm^3/molecule·s. The B3LYP/RCEP60VDZ overpredicts the rate constant at 3.49×10^{-12} cm^3/molecule·s. For the reverse unimolecular decomposition, no experimental data exist, but there have been two previous investigations with one based upon ab initio calculations and QCT,[4] while the other carried out RRKM theory using the Master Equation formalism.[9] The rate constant prediction of the current work calculated at the CCSD(T)/AVTZ level of theory (0.154 1/s) agreed best with the calculations carried out using QCT methods of Shepler et al.[4] (0.48 1/s), deviating by a factor of approximately 3. Again, the B3LYP/RCEP60VDZ level of theory overpredicts the rate constant with a value of 0.846 1/s. For this reaction, it is interesting to note that the B3LYP/RCEP60VDZ level of theory most accurately predicts the R1 enthalpy change at 298.15 K with a deviation of 0.21 kcal/mol, but the CCSD(T)/AVTZ level of theory most accurately predicts the frequency and geometry data for HgBr and deviates from the experimental enthalpy of reaction by only 0.77 kcal/mol.

For R2, the B3LYP/RCEP60VDZ level of theory agreed best with the previous theoretical predictions for the forward and reverse rate constant. It is important to note that this level of theory performed best for the heat of reaction prediction as well, underpredicting by 0.73 kcal/mol. Balabanov et al.[14] used ab initio calculations with QCT methods, transition state theory with the canonical variation theory implementation (CVT), improved canonical variational theory (ICVT), and microcanonical variational theory (μVT) to arrive at $3.4 \pm 0.15 \times 10^{-31}$, 5.4×10^{-31}, 4.6×10^{-31}, and 3.9×10^{-31} cm^3/molecule·s for the forward rate constant, respectively. The prediction in the current work at the B3LYP/RCEP60VDZ level of theory using VTST is 1.65×10^{-31} cm^3/molecule·s, agreeing best with the QCT calculations of Balabanov et al.,[14] underpredicting the rate by about a factor of 2. There is only one experimental study available for this reaction, carried out by Ariya et al.[7] and estimates a forward rate constant of $0.9 \pm 0.2 \times 10^{-16}$ cm^3/molecule·s. This rate constant is approximately 15 orders of magnitude faster than the five theoretical predictions previously discussed. Within their study, they report the use of halocarbon wax to coat their reactor surface to prevent heterogeneous surface interactions for Hg oxidation; however, it is clear from this discrepancy that surface interactions are occurring in their experimental setup and playing a significant role in enhancing Hg oxidation via bromine. Within their work, Ariya et al.[7] acknowledged the

Table 3. Comparison of Rate Constant Predictions (cm^3/molecule·s) to Available Theoretical and Experimental Data at 298.15 K

	B3LYP/[1]ECP60MDF; [2]RCEP60VDZ	CCSD(T)/ AVTZ	other theory	experiment
R1 Hg + Br ↔ HgBr	[2]3.49 (−12)	6.38 (−13)	9.8 (−13)[a] 2.0 (−12)[b] 1.1 (−12)[b] 3.0 (−13); 9.7 (−13)[d] 3.2 (−12)[e]	3.6 ± 1.8 (−13)[f]
R1 HgBr ↔ Hg + Br	[2]0.846	0.154	0.48[a] 0.007[c]	NA
R2 Hg + Br_2 ↔ HgBr + Br	[2]1.65 (−31)	6.03 (−29)	3.4 ± 0.15 (−31); 5.4 (−31); 4.6 (−31); 3.9 (−31)[g]	0.9 ± 0.2 (−16)[e]
R2 HgBr + Br ↔ Hg + Br_2	[2]2.20 (−12)	2.29 (−10)	3.89 ± 0.17 (−11); 6.15 (−11); 5.30 (−11); 4.52 (−11)[g]	NA
R4 HgBr + Br ↔ $HgBr_2$	[1]1.78 (−13)	5.31 (−12)	2.98 ± 0.14 (−11); 1.27 (−10); 1.22 (−10); 1.05 (−10)[g] 2.50 (−10)[c]	NA
R4 $HgBr_2$ ↔ HgBr + Br	[1]2.47 (−40)	7.37 (−39)	5.50 ± 0.26 (−39); 2.40 (−38); 2.30 (−38); 2.00 (−38)[g]	NA

[a] Reference 4. [b] Reference 5. [c] Reference 9. [d] Reference 6. [e] Reference 7. [f] Reference 8. [g] Reference 14. Numbers in parentheses represent powers of 10.

Table 4. Transition Structure Geometry for R1 and R4

	HgBr	HgBr	BrHgBr	BrHgBr
level of theory	CCSD(T)/ AVTZ	B3LYP/RCEP60VDZ	CCSD(T)/ AVTZ	B3LYP/ECP60MDF
bond length (Å) Hg−Br	4.10	4.40	2.47	2.50
bond length (Å) Hg−Br			4.00	4.20
bond angle (deg)	180	180	180	180

Table 5. Transition Structure Geometry for R2 and R3

	HgBrBr	HgBrBr	HgBrH
level of theory	CCSD(T)/ AVTZ	B3LYP/RCEP60VDZ	B3LYP/RCEP60VDZ
bond length (Å) Hg−Br	2.50	2.68	2.72
bond length (Å) Br−Br; Br−H	3.50	3.58	2.61
bond angle (deg)	180	180	180

issues experienced with the use of this wax coating and the difficulty associated with establishing conditions to prevent significant surface effects. For the reverse reaction, there are no experimental data for comparison, but theoretical predictions from Balabanov et al.[14] are available. The rate constant prediction of the current work at the B3LYP/RCEP60VDZ level of theory is approximately an order of magnitude slower than the predictions of Balabanov et al.[14] at 2.2×10^{-12} cm^3/molecule·s. The CCSD(T)/AVTZ level of theory overpredicts the rate constant for both forward and reverse directions of R2 and also overpredicts the heat of reaction by 2.03 kcal/mol.

For the forward and reverse rate constants of R4, no experimental data exists, but theoretical predictions of Balabanov et al.[14] as well as Goodsite et al.[9] exist for comparison to the current work. For the forward rate constant prediction, the

Table 6. Transition Structure Geometry for R5 and R6 Carried out at the CCSD(T)/AVTZ and B3LYP/ECP60MDF Levels of Theory, Respectively

	BrHgBrBr	BrHgBrH
bond length (Å) (Br−Hg)−Br−X	2.47	2.54
bond length (Å) Br−(Hg−Br)−X	5.75	2.50
bond length (Å) Br−Hg−(Br−X)	2.33	2.10
bond angle (deg)	180	180

CCSD(T)/AVTZ level of theory predicts a slower rate constant (5.31×10^{-12} cm^3/molecule·s) compared to the prediction of Goodsite et al.[9] (2.50×10^{-10} cm^3/molecule·s) and agrees best with the value from Balabanov et al. ($2.98 \pm 0.14 \times 10^{-11}$

Table 7. Theoretical Activation Barriers (kcal/mol) and Preexponential Factors (cm^3/mol·s) for Hg Oxidation Reactions

	forward		reverse			
level of theory	E_a (kcal/mol)	A (cm^3/mol·s)	E_a (kcal/mol)	A (cm^3/mol·s)	level of theory	K_{eq}[c]
R1 Hg + Br ↔ HgBr	0.859[a]	4.00 (11)	15.64	4.57[b] (10)	CCSD(T)/AVTZ	1.00 (8)
	1.912[a]	2.00(12)	14.58	4.18 (10)	B3LYP/RCEP60VDZ	4.83 (−21)
R2 Hg + Br_2 ↔ HgBr + Br	26.49	9.76 (14)	∼0	1.38 (14)	CCSD(T)/AVTZ	4.83 (−21)
	30.08	1.15 (15)	2.32	6.65 (13)	B3LYP/RCEP60VDZ	
R3 Hg + HBr ↔ HgBr + H	71.58	1.86 (13)	4.92	3.65 (12)	B3LYP/RCEP60VDZ	4.37 (−52)
R4 HgBr + Br ↔ $HgBr_2$	9.18[a]	2.00 (12)	62.81	8.62[b] (7)	CCSD(T)/AVTZ	6.28 (−47)
	7.644[a]	8.00 (10)	64.36	3.97[b] (7)	B3LYP/ECP60MDF	
R5 HgBr + Br_2 ↔ $HgBr_2$ + Br	0.87	4.02 (11)	24.5	4.30 (12)	CCSD(T)/AVTZ	1.30 (−18)
R6 HgBr + HBr ↔ $HgBr_2$ + H	18.68	9.41 (12)	3.57	1.16 (15)	B3LYP/ECP60MDF	6.91 (−14)

[a] The temperature-dependent rate expression for the forward reaction of R1 and R4 is $k = A(T/298)^{-n}$ with n listed in the E_a column. [b] Units of A for the unimolecular R1 and R4 are 1/s. [c] Reference 28. Numbers in parentheses represent powers of 10.

molecule·s), while still deviating by an order of magnitude. For the unimolecular direction of R4, again, the CCSD(T)/AVTZ level of theory agrees best, and falls in the range of previous theoretical estimates[14] ($5.5 \pm 0.26 \times 10^{-39}$ cm^3/molecule·s). The use of this level of theory is further validated by the agreement to the experimental enthalpy of reaction, with an overprediction of just 0.08 kcal/mol.

From these comparisons of reactant/product geometries, heats of reaction, and kinetics at 298.15 K to previous experimental and theoretical data available in the literature, the most appropriate levels of theory have been employed to carry out kinetic predictions for the forward and reverse directions of R3, R5, and R6 for implementation into postcombustion Hg oxidation models involving bromine.

Potential energy surfaces (PES) have been generated for R2, R3, R5, and R6 at multiple levels of theory and selected images are shown in Figures 1−4, respectively. Potential curves for the unimolecular decomposition R1 and R4 were constructed, but are omitted here. Geometries of R1 and R4 transition structures at both CCSD(T)/AVTZ and B3LYP/RCEP60VDZ are listed in Table 4. Each of the potential energy surfaces were also created at two levels of theory, i.e., (1) using the B3LYP method with the basis set that provided the best agreement with the experimental heat of reaction and (2) at the CCSD(T)/AVTZ level of theory because of the agreement to experimental geometry, vibrational frequency, and heats of reaction data. Figure 1 shows the PES for R2 at the B3LYP/RCEP60VDZ level of theory. A linear reaction path was assumed and the activated Hg−Br−Br complex exhibiting one imaginary frequency was found to have an Hg−Br interaction distance of 2.68 Å and a Br−Br distance of 3.58 Å, as shown in Table 5. At the CCSD(T)/AVTZ level of theory, the activated complex geometry was fairly more contracted with an Hg−Br distance of 2.50 Å and a Br−Br distance of 3.5 Å.

Figure 2 shows the PES for R3 at the B3LYP/RCEP60VDZ level of theory and again with a linear reaction path assumed with the activated Hg−Br−H complex having an Hg−Br interaction distance of 2.72 Å and a Br−H distance of 2.61 Å, as shown in Table 5. Figure 3 shows the PES for R5 at the CCSD(T)/AVTZ level of theory with an activated Br−Hg−Br−Br complex. The Br−Hg bond distance was held constant in the transition state calculation at 2.47 Å, which is closer to the equilibrium distance of the product $HgBr_2$ (2.4 Å) versus that of the reactant HgBr (2.7 Å). Various Br−Hg distances were tested with this distance resulting in the minimum rate constant. The activated complex exhibiting one imaginary frequency had a Br−Br interaction distance of 2.33 Å and an Hg−Br distance of 5.75 Å. Figure 4 shows the PES of R6 at the B3LYP/ECP60MDF level of theory with an activated Br−Hg−Br−H linear complex. The Br−Hg bond distance was held constant at 2.55 Å, which is a weighted average of the optimized HgBr (2.64 Å) and $HgBr_2$ (2.46 Å) bond distances, due to the higher electronegativity of Br in contrast to H. The activated complex exhibiting one imaginary frequency had a Hg−Br interaction distance of 2.50 Å and a Br−H distance of 2.10 Å. In future work, this reaction will be treated more rigorously since it is likely by testing different configurations as was done with the other three bimolecular reactions, that a smaller rate may be obtained. The activated complex geometries of R5 and R6 are available in Table 6.

Table 7 presents the forward and reverse kinetic data including activation energies in kilocalories per mole, and preexponential factors in cubic centimeters per mole second and inverse seconds, for bimolecular and unimolecular reactions, respectively. For the atom−radical recombination R1 and radical−radical recombination R4 reactions, the rate constants were found to decrease with increasing temperature. These rate constants could still be expressed in an Arrhenius fashion, but it would require a negative activation energy to capture the trend accurately. Both reactions are nearly barrierless in the forward direction. Increasing the temperature provides increased energy to an activated complex, making it less likely for the complex to proceed to the potential well through the product channel. The rate expressions for these reactions are represented by a power law expression, e.g., $k = A(T/298)^{-n}$ to accurately capture the negative temperature dependence.

Although it is difficult to conclude how the concentration profiles of mercury and its oxidized forms will change as a function of the temperature quenching representative of postcombustion flue gas without their inclusion into a global combustion model, some indications of reaction behavior can be inferred from the predicted rate constants. For instance, the fastest of all the reactions is the unimolecular decomposition R1 of HgBr, as indicated in Table 3 when compared to other rate constants at ambient conditions. For the forward of R3, it is clear from the very small (e.g., 4.37×10^{-47}) equilibrium constant that the reactants are favored over the products, yet the forward activation barrier is quite high. So, although the forward direction of R3 will

be thermodynamically favored, it will likely be kinetically limited. A direct comparison can be made between the competing $HgBr_2$ formation pathways of R5 (via Br_2) and R6 (via HBr). From the equilibrium constants, the products of R6 are thermodynamically favored over those of R5, while the kinetics of R5 are favored over those of R6. This implies that both formation pathways are likely. Finally, the reactions with low activation barriers, i.e., forward of R5, reverse of R2, reverse of R3, and the reverse of R6, are likely to depend weakly on temperature.

Upon the basis of a thorough comparison of geometry, vibrational frequency, heats of reaction, and available kinetic data, the most reliable predicted kinetic data are available in Table 7. It is suggested that these data are used for implementation into postcombustion flue gas modeling of mercury oxidation reactions involving bromine. These data are intended for use over a broad temperature range spanning the conditions of postcombustion flue gases in order to more accurately determine trace metal speciation, which will aid in the design of more effective control technologies for these volatile and environmentally harmful compounds.

AUTHOR INFORMATION

Corresponding Author

*Tel.: 650-724-9449. Fax: 650-725-2099. E-mail: jen.wilcox@stanford.edu.

ACKNOWLEDGMENT

The computations were carried out on the Center for Computational Earth & Environmental Science (CEES) cluster in the School of Earth Sciences at Stanford University. Dennis Michael is gratefully acknowledged for the installation of Molpro on CEES and for his administration assistance.

REFERENCES

(1) United States Environmental Protection Agency, 2005 Clean Air Interstate Rule. http://www.epa.gov/interstateairquality (accessed July 2008).

(2) Vosteen, B. W.; Kanefke, R.; Koser, H. Bromine-Enhanced Mercury Abatement from Combustion Flue Gases - Recent Industrial Applications and Laboratory Research. *VGB PowerTech* **2006**, *86*, 70.

(3) Liu, S.; Yan, N.; Liu, Z.; Qu, Z.; Wang, H. P.; Chang, S.; Miller, C. Using Bromine Gas to Enhance Mercury Removal from Flue Gas of Coal-Fired Power Plants. *Environ. Sci. Technol.* **2007**, *41*, 1405–1412.

(4) Shepler, B. C.; Balabanov, N. B.; Peterson, K. A. Hg+ Br → HgBr recombination and collision-induced dissociation dynamics. *J. Chem. Phys.* **2007**, *127*, 164304.

(5) Khalizov, A. F.; Viswanathan, B.; Larregaray, P.; Ariya, P. A. A Theoretical Study on the Reactions of Hg with Halogens: Atmospheric Implications. *J. Phys. Chem. A* **2003**, *107*, 6360.

(6) Spicer, C. W., Satola, J., Abbgy, A. A., Plastridge, R. A., Cowen, K. A., *Kinetics of Gas-Phase Elemental Mercury Reactions with Halogen Species, Ozone, and Nitrate Radical under Atmospheric Conditions*; Florida Department of Environmental Protection: 2002.

(7) Ariya, P. A.; Khalizov, A.; Gidas, A. Reactions of Gaseous Mercury with Atomic and Molecular Halogens: Kinetics, Product Studies, and Atmospheric Implications. *J. Phys. Chem. A* **2002**, *106*, 7310.

(8) Donohoue, D. L.; Bauer, D.; Cossairt, B.; Hynes, A. J. Temperature and pressure dependent rate coefficients for the reaction of Hg with Br and the reaction of Br with Br: a pulsed laser photolysis-pulsed laser induced fluorescence study. *J. Phys. Chem. A* **2006**, *110*, 6623–6632.

(9) Goodsite, M. E.; Plane, J. M. C.; Skov, H. A Theoretical Study of the Oxidation of Hg^0 to $HgBr_2$ in the Troposphere. *Environ. Sci. Technol.* **2004**, *38*, 1772.

(10) Kreevoy, M. M., Truhlar, D. G., Transition State Theory. *Investigation of Rates and Mechanisms of Reactions*, Bernasconi, C. F., Ed.; Wiley: New York, 1986; Vol. 6, p 14.

(11) Gilbert, R. G., Smith, S. C. *Theory of Unimolecular and Recombination Reactions*; Blackwell: Oxford, 1990.

(12) Becke, A. D. Density-Functional Thermochemistry 3. The Role of Exact Exchange. *J. Chem. Phys.* **1993**, *98*, 5648.

(13) Stephens, P. J.; Devlin, F. J.; Chabalowski, C. F.; Frisch, M. J. Ab Initio Calculation of Vibrational Absorption and Circular Dichroism Spectra using Density Functional Force Fields. *J. Phys. Chem.* **1994**, *98*, 11623.

(14) Balabanov, N. B.; Shepler, B. C.; Peterson, K. A. Accurate global potential energy surface and reaction dynamics for the ground state of $HgBr_2$. *J. Phys. Chem. A* **2005**, *109*, 8765–8773.

(15) Wener, H. J., Knowles, P. J. *MOLPRO*, version 2002.6, a package of ab initio programs; http://www.molpro.net.

(16) Purvis, G. D. I.; Bartlett, R. J. A full coupled-cluster singles and doubles model: The inclusion of disconnected triples. *J. Chem. Phys.* **1982**, *76*, 1910.

(17) Raghavachari, K.; Trucks, G. W.; Pople, J. A.; Head-Gordon, M. A fifth-order perturbation comparison of electron correlation theories. *Chem. Phys. Lett.* **1989**, *157*, 479.

(18) Watts, J. D.; Gauss, J.; Bartlett, R. J. Coupled-Cluster Methods with Non-Iterative Triple Excitations for Restricted Open-shell Hartree-Fock and Other General Single Determinant Reference Functions. Energies and Analytical Gradients. *J. Chem. Phys.* **1993**, *98*, 8718.

(19) Peterson, K. A.; Puzzarini, C. Systematically convergent basis sets for transition metals. II. Pseudopotential-based correlation consistent basis sets for the group 11 (Cu, Ag, Au) and 12 (Zn, Cd, Hg) elements. *Theor. Chem. Acc.* **2005**, *114*, 283.

(20) Peterson, K. A.; Figgen, D.; Goll, E.; Stoll, H.; Dolg, M. Systematically convergent basis sets with relativistic pseudopotentials. I. Correlation consistent basis sets for the post-*d* group 13−15 elements. *J. Chem. Phys.* **2003**, *119* (21), 11113.

(21) Figgen, D.; Rauhut, G.; Dolg, M.; Stoll, H. Energy-consistent pseudopotentials for group 11 and 12 atoms: adjustment to multi-configuration Dirac−Hartree−Fock data. *Chem. Phys.* **2005**, *311*, 227–244.

(22) Hay, P. J.; Wadt, W. R. *Ab initio* effective core potentials for molecular calculations. Potentials for K to Au including the outermost core orbitals. *J. Chem. Phys.* **1985**, *82*, 299.

(23) Stevens, W. J.; Krauss, M. Relativistic compact effective potentials and efficient, shared-exponent basis sets for third-, fourth-, and fifth-row atoms. *Can. J. Chem.* **1992**, *70*, 612.

(24) Krishnan, R.; Binkley, J. S.; Seeger, R.; Pople, J. A. Self-consistent molecular orbital methods. XX. A basis set for correlated wave functions. *J. Chem. Phys.* **1980**, *72*, 650.

(25) Holbrook, K. A., Pilling, M. J., Robertson, S. H. *Unimolecular Reactions*, second ed.; Wiley: Chichester, UK, 1996. p 126.

(26) Laidler, K. J. *Chemical Kinetics*, third ed.; Harper and Row: New York, 1987.

(27) Beyer, T.; Swinehart, D. F. Algoritm 448. Number of Muliple-Restricted Partitions [A1]. *Commun. ACM* **1973**, *16*, 379.

(28) Chase, M. W. *NIST-JANAF Thermochemical Tables*; 1998; Vol. 1, p 1952.21.

(29) Wigner, E. Crossing of potential thresholds in chemical reactions. *Z. Phys. Chem. B* **1932**, *19*, 203.

(30) Coxon, J. A.; Hajigeorgiou, P. G. Isotopic Dependence of Born-Oppenheimer Breakdown Effects in Diatomic Hydrides: The X $^1\Sigma^+$ States of HI/DI and HBr/DBr. *J. Mol. Spectrosc.* **1991**, *150*, 1–27.

(31) Huber, K. P., Herzberg, G. In *Molecular Spectra and Molecular Structure IV. Constants of Diatomic Molecules*; Van Nostrand: Princeton, NJ, 1979.

(32) Focsa, C.; Li, H.; Bernath, P. F. Characterization of the Ground State of Br_2 by Laser-Induced Fluorescence Fourier Transform Spectroscopy of the B $^3\Pi_0{}^{+u}$-X $^1\Sigma^{+g}$ System. *J. Mol. Spectrosc.* **2000**, *200*, 104–119.

(33) Tellinghuisen, J.; Ashmore, J. G. The B → X Transition in $^{200}Hg^{79}Br$. *Appl. Phys. Lett.* **1982**, *40*, 867–869.

(34) Deyanov, R. Z.; Petrov, K. P.; Ugarov, V. V.; Shchedrin, B. M.; Rambidi, N. G. Automatic background subtraction in gas electron diffraction: The covariance matrix in least-squares structure-parameter analysis. *Zh. Strukt. Khim.* **1985**, *26* (5), 58.

(35) Nishimiya, N.; Yukiya, T.; Ohtsuka, T.; Suzuki, M. Laser Spectroscopy of Vibration-Rotation Lines in the 3 ← 0, 5 ← 0, and 6 ← 0 Overtones of HBr. *J. Mol. Spectrosc.* **1997**, *182*, 309–314.

(36) Braune, H.; Engelbrecht, G. *Z. Phys. Chem. Abt. B* **1932**, *19*, 303.

(37) Beattie, I. R.; Horder, J. R. Gas-phase Raman spectra of some dihalides of zinc and mercury, of '$GaCl_2$' and $GaCl_2Br$ and $GaBr_2Cl$. *J. Chem. Soc. A* **1970**, *14*, 2433.

(38) Sponer, H.; Teller, E. Electronic spectra of polyatomic molecules. *Rev. Mod. Phys.* **1941**, *13*, 75.

(39) Clark, R. J. H.; Rippon, D. M. Vapour phase Raman spectra of mercury(II) chloride, mercury(II) bromide and mercury(II) iodide. $\nu_1(\Sigma_{g^+})$ band contours and the mercury-halogen bond polarisability derivatives. *J. Chem. Soc., Faraday Trans. 2* **1973**, *69*, 1496.

(40) Malt'sev, A. A.; Selivanov, G. K.; Yampolsky, V. I.; Zavalishin, N. I. Far Infrared Absorption Spectra of Mercury Dihalide Vapours. *Nat. Phys. Sci.* **1971**, *231*, 157.

(41) Klemperer, W.; Lindeman, L. Infrared Spectrum of Mercuric Chloride and Bromide. *J. Chem. Phys.* **1956**, *25*, 397.

(42) Balabanov, N. B.; Peterson, K. A. Mercury and Reactive Halogens: The Thermochemistry of Hg + {Cl_2, Br_2, BrCl, ClO, and BrO}. *J. Phys. Chem. A* **2003**, *107*, 7465–7470.

(43) Ariya, P. A.; Dastoor, A. P.; Amyot, M.; Schroeder, W. H.; Barrie, L.; Anlauf, K.; Raofie, F.; Ryzhkov, A.; Davignon, D.; Lalonde, J.; Steffen, A. The Arctic: a sink for mercury. *Tellus B* **2004**, *56* (5), 397–403.

(44) Stein, S. E. IR and Mass Spectra. *NIST Chemistry WebBook*; Mallard, W. G., Linstrom, P. J., Eds.; NIST Standard Reference Database Number 69; National Institute of Standards and Technology: Gaithersburg, MD, (February) 2000; 1,2-ethanediol (http://webbook.nist.gov).

(45) Cox, J. D., Wagman, D. D., Medvedev, V. A. In *CODATA key values for thermodynamics*; Hemisphere Publ. Co.: New York, 1989.

(46) Lide, D. R., Ed. *CRC Handbook of Chemistry and Physics*; Taylor and Francis: Boca Raton, FL, 2007; Vol. internet version 2007.